
**Pacific Northwest
National Laboratory**

Operated by Battelle for the
U.S. Department of Energy

Long Wave Infrared Cavity Enhanced Sensors

M. S. Taubman

B. D. Cannon

T. L. Myers

C. A. Bonebrake

P. M. Aker

J. F. Schultz

October 2003

Prepared for the U.S. Department of Energy
under Contract DE-AC06-76RL01830



DISCLAIMER

This report was prepared as an account of work sponsored by an agency of the United States Government. Neither the United States Government nor any agency thereof, nor Battelle Memorial Institute, nor any of their employees, makes **any warranty, express or implied, or assumes any legal liability or responsibility for the accuracy, completeness, or usefulness of any information, apparatus, product, or process disclosed, or represents that its use would not infringe privately owned rights.** Reference herein to any specific commercial product, process, or service by trade name, trademark, manufacturer, or otherwise does not necessarily constitute or imply its endorsement, recommendation, or favoring by the United States Government or any agency thereof, or Battelle Memorial Institute. The views and opinions of authors expressed herein do not necessarily state or reflect those of the United States Government or any agency thereof.

PACIFIC NORTHWEST NATIONAL LABORATORY
operated by
BATTELLE
for the
UNITED STATES DEPARTMENT OF ENERGY
under Contract DE-AC06-76RL01830

Printed in the United States of America

Available to DOE and DOE contractors from the
Office of Scientific and Technical Information,
P.O. Box 62, Oak Ridge, TN 37831-0062;
ph: (865) 576-8401
fax: (865) 576-5728
email: reports@adonis.osti.gov

Available to the public from the National Technical Information Service,
U.S. Department of Commerce, 5285 Port Royal Rd., Springfield, VA 22161
ph: (800) 553-6847
fax: (703) 605-6900
email: orders@ntis.fedworld.gov
online ordering: <http://www.ntis.gov/ordering.htm>



This document was printed on recycled paper.

Long Wave Infrared Cavity Enhanced Sensors

M. S. Taubman
B. D. Cannon
T. L. Myers
C. A. Bonebrake
P. M. Aker
J. F. Schultz

October 2003

Prepared for
the U.S. Department of Energy
under Contract DE-AC06-76RLO 1830

Pacific Northwest National Laboratory
Richland, Washington 99352

Summary

The principal goal of Pacific Northwest National Laboratory's (PNNL's) long wave infrared (LWIR) cavity enhanced sensor (CES) project is to explore ultra-sensitive spectroscopic techniques and apply them to the development of LWIR chemical sensors needed for detecting signs of weapons proliferation and/or terrorist activities. This includes detecting not only the weapons of mass destruction (WMDs) themselves, but also signatures of their production and/or detonation. The LWIR CES project is concerned exclusively with developing point sensors; other portions of PNNL's IR Sensors program address stand off detection. PNNL's LWIR CES research is distinguished from that done by others by the use of quantum cascade lasers (QCLs) as the light source. QCLs are novel devices, and a significant fraction of our research has been devoted to developing the procedures and hardware required to implement them most effectively for chemical sensing. This report details the progress we have made on our LWIR CES sensor development.

During FY02, PNNL investigated several LWIR CES implementations including direct cavity-enhanced detection (called simple CES), cavity-dithered phase-sensitive detection (called FM recovery CES) and resonant sideband cavity-enhanced detection (called noise immune cavity enhanced optical heterodyne molecular spectroscopy, NICE-OHMS). Considerable theoretical analysis was performed to ensure that we clearly understood the operation of each of these sensor architectures, with estimates of the detection limits (given in terms of absorption sensitivity) being compared with experimental values in each case. All of these techniques looked promising for further development, with simple CES being the easiest to implement and operate while offering limited sensitivity, through to NICE-OHMS, promising the best sensitivity with an accompanying increase in complexity. The sensitivity of our NICE-OHMS apparatus was confirmed to be $9.7 \times 10^{-11} \text{ cm}^{-1} (\text{Hz})^{-1/2}$, which is within a factor of 20 of the theoretical shot noise limit of $4.9 \times 10^{-12} \text{ cm}^{-1} (\text{Hz})^{-1/2}$.

In FY03 several equipment upgrades identified as necessary in FY02 were implemented. These included increased cavity finesse, which in theory leads directly to improved sensitivity, and various electronic and mechanical improvements allowing increased control and signal to noise. Several limitations surfaced that helped guide our choice for both the most suitable spectroscopic technique and the sensor architecture for immediate development into a fieldable technology. It was found that by increasing the optical cavity finesse, the intra-cavity power also increased to the point where the analyte became highly saturated. This manifested itself by greatly reducing the signals observed when using the narrow sub-Doppler features (Lamb dips) we had been using. This was unexpected, and careful measurements and comparisons to theory were made to confirm that this was indeed what was happening. The question of whether the saturation behavior could be leveraged, or compensated for in a sensor was also carefully examined as discussed later in this report. The conclusion reached was that Doppler-limited spectroscopy should be chosen over of sub-Doppler for the PNNL prototype fieldable LWIR CES.

Another discovery was the surprising reduction in the response of our LWIR mercury-cadmium-telluride (MCT) detectors at the operating frequency of the NICE-OHMS architecture. This, combined with previously known limitations pertaining to the modulation characteristics of the QCL were using,

caused us to decide in favor of the FM recovery CES for prototype development rather than NICE-OHMS. This decision was based not on any conclusion that NICE-OHMS was not a viable technique, but rather that a fieldable sensor can be pursued almost immediately using other techniques while allowing more fundamental research to continue on applying NICE-OHMS to the LWIR. Because of these findings, we propose that our FY04 activities focus on the development of a prototype LWIR CES based on the FM recovery technique and Doppler-limited spectroscopy, while basic research on NICE-OHMS continues.

Contents

Summary	iii
1.0 Introduction	1.1
1.1 Description of Various Sensors under Investigation	1.1
1.2 Achievements in FY03 in Light of FY02 Goals	1.4
1.2.1 Construction of Better Optical Cavities	1.4
1.2.2 Implementation of Amplitude Stabilization to Reduce Optical Fringing Effects ..	1.4
1.2.3 Exploring the Limitations of Increasing Cavity Finesse	1.5
1.3 Progress Independent of FY02 Goals.....	1.5
2.0 Saturation.....	2.1
2.1 The Impact of Saturation.....	2.1
2.2 The Nature of Saturation	2.2
2.3 The Effects of Saturation on Strength and Depth of Absorption Features.....	2.3
2.4 The Effect of Saturation on Homogeneously Broadened Intra-Cavity Absorption Features	2.4
2.5 Sub-Doppler Absorption Features and the Lamb Dip.....	2.7
2.6 Effect of Saturation on Sub-Doppler Intra-Cavity Absorption Features.....	2.8
2.7 Conclusions about the Impact of Saturation on Sensor Performance	2.11
3.0 Mercury-Cadmium-Telluride Detectors	3.1
3.1 Detectors in the LWIR	3.1
3.2 Transfer Function Measurements.....	3.4
3.3 Falling Responsivity.....	3.6
3.4 Optical Fringing	3.7
3.5 Other approaches and Other Detectors.....	3.8
4.0 QCL Modulation Characteristics.....	4.1
4.1 Modulating QCLs.....	4.1
5.0 FY04 Plans - A Fieldable Sensor.....	5.1
6.0 References	6.1
Appendix A - Further Work for FY03 - Taken From the FY02 Report	A.1
Appendix B - Frequency Control Loop in NICE-OHMS Experiments.....	B.1

Figures

1.1 Cavity-Stabilized QCL Used as a Chemical Sensor	1.2
1.2 FM Recovery Cavity-Enhanced Sensor.....	1.2
1.3 NICE-OHMS Recovery Sensor.....	1.4
2.1a Absorption and Saturation Functions for Peak Saturation Parameter of 1.0	2.4
2.1b Absorption and Saturation Functions for Peak Saturation Parameter of 0.3	2.4
2.2. Narrowing Due to Saturation as Compared to an Unsaturated Profile of Equivalent Depth is Shown	2.6
2.3a 3-D Plot of the Narrowing of the Saturated Intra-Cavity Doppler Feature as Compared to the Width of an Unsaturated Feature of Equivalent Depth.....	2.6
2.3b 3-D Plot of the Cavity Intensity Function p vs. Absorption Factor and Empty Cavity Saturation	2.6
2.4 Lamb Dips for Absorption Profiles with Various Saturation Levels.....	2.8
2.5 Iterative Solution of Intra-Cavity Lamb Dip Problem.....	2.9
2.6 A sequence of intra-cavity Lamb dips solved using the iterative technique described above...	2.9
2.7 Lamb Dip Size Relative to Unsaturated Inhomogeneous Feature and Relative to Saturated Features	2.10
2.8 Lamb Dip Width as a Function of Empty Cavity Saturation for Various Absorption Factors..	2.11
3.1 Measured Impedance Function and Modeled Impedance Function of a 100 Micron Diameter MCT Detector	3.2
3.2 Circuit Approximating MCT Detector with Poor High Frequency Connections	3.3
3.3 Measured Impedance Function and Modeled Impedance Function of the New 100 Micron Diameter Close-Coupled MCT Detector.....	3.3
3.4 Relative Simple Model of the New 100 Micron MCT Detectors with Close Connections.....	3.4

3.5	Transfer Function Response of Simulated Detector and Preamplifier Combination, as Compared to the Theoretical Response of an Ideal Detector and Transimpedance Amplifier as Shown in Figure 3.6.....	3.4
3.6	Simplest Form of Detector and Transimpedance Preamplifier and the Equivalent Impedance Circuit	3.5
3.7	Comparison of Heterodyne Measurements of Detector-Preamplifier Response Using Both Old and Close-Coupled Detectors.....	3.7
3.8	Results of Direct Transmission Cavity-Enhanced Sensor	3.8
4.1.	Log-Log Plot Showing the Phase Modulation in Radians of the QCL vs. Frequency in MHz for a 20 dBm RF Drive.....	4.2

1.0 Introduction

The FY02 report on LWIR cavity-enhanced sensors was written with the intention of giving both an overview of the status of this technology at PNNL at that time, and an in-depth scientific explanation of the theory and operation of cavity-enhanced techniques, modulation and signal recovery, and the noise-immune technique of resonant-sideband detection (NICE-OHMS). As such, this document represents a full and detailed explanation of the theory behind the work being performed in CW cavity-enhanced sensing at PNNL, and thus is a significant document. To this end, the FY02 report is referenced where in-depth technical explanations are required.

1.1 Description of Various Sensors under Investigation

Various CES architectures and results were discussed in FY02. A brief summary of their operation is given here as preparation for what is to follow. The reader should refer to the FY02 report for a more thorough understanding of their operation.

The most basic cavity-enhanced sensor we use is shown in Figure 1.1. It is referred to as the “Simple Cavity-Enhanced Sensor” because it is based on direct transmission through the optical cavity, without the use of any modulation technique other than that involved in locking the laser to the optical cavity. The optical field from a quantum cascade laser (QCL) is coupled into an optical cavity via an acousto-optic modulator (AOM) and a Faraday isolator in order to minimize the optical feedback into the QCL from back reflections. Reflected and transmitted light from the cavity are observed using detectors D1 and D2 respectively. The QCL is locked to the optical cavity using the Pound-Drever-Hall (PDH) technique, the electronics for this being compressed into one block called “stabilization electronics.” The optical cavity also forms a chamber allowing an analyte to be introduced at low pressures. A piezoelectric element in contact with the transmission mirror allows the optical cavity length to be scanned, thus changing the cavity mode frequencies and that of the QCL since it is locked to one of these modes. As the frequency of the sensor is scanned, the signal from detector D2, is filtered at some bandwidth B, measured on an oscilloscope and then recorded.

The advantages of this sensor are that the operation of the sensor is relatively simple, and it gives a direct result that can exactly be modeled mathematically. We have also found it to be extremely useful for characterizing absorption and saturation values, as will be discussed later. The disadvantages are that the sensitivity is directly limited by the low frequency amplitude noise of the laser and detector, specifically, $1/f$ noise.

The next kind of sensor we use is the “FM Recovery Cavity-Enhanced Sensor” (Figure 1.2). Here, a modulation technique is added to allow the low frequency noise limitations to be overcome. Again, the QCL is locked to the peak of the cavity mode and the cavity length is scanned or swept to move both mode and laser frequency across molecular absorption features. The difference is that in addition to being scanned, the cavity length is also rapidly “dithered” using a modulation frequency in the 10s of kHz. This cavity modulation signal (independent of that applied to the laser in order to lock it to the

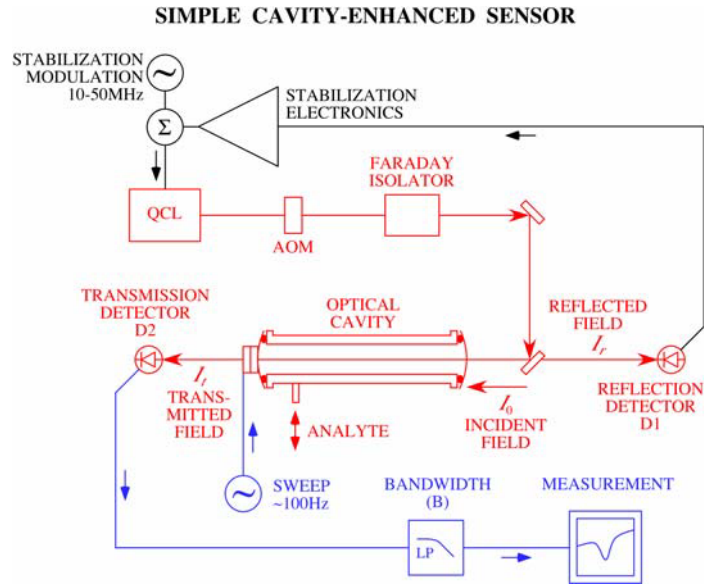


Figure 1.1. Cavity-Stabilized QCL Used as a Chemical Sensor. Absorption due to the intra-cavity analyte causes dramatic changes in the cavity transmission. Optical elements are in red, stabilization in black, measurement electronics in blue. Incident, reflected and transmitted cavity fields of intensities I_0 , I_r and I_t are indicated.

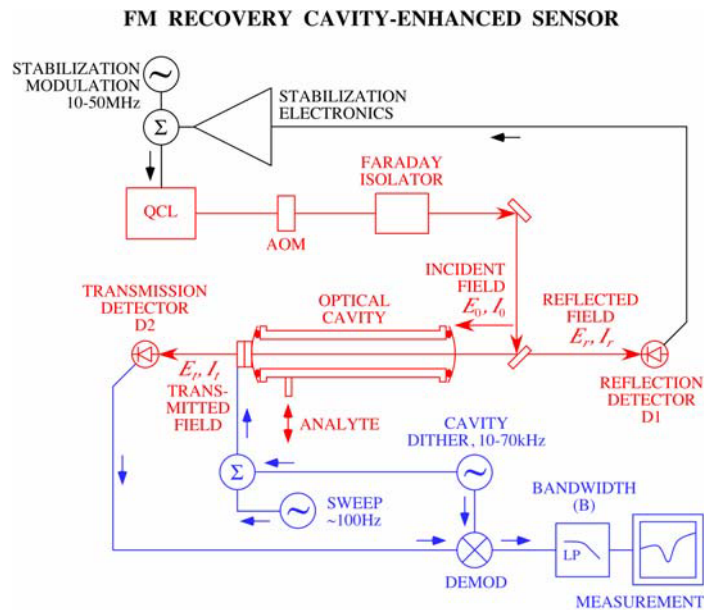


Figure 1.2. FM Recovery Cavity-Enhanced Sensor. The QCL is locked to the cavity as before. However, in addition to the cavity length being scanned, it is also dithered or modulated. The transmission signal from D2 is demodulated accordingly, then filtered and recorded as before. Intensities and electric field amplitudes are indicated for incident, reflected and transmitted fields.

cavity,) is applied directly to the piezoelectric element in addition to the signal used to produce the frequency sweep. Since this modulation frequency is well within the bandwidth of the laser-locking loop, the laser frequency follows this cavity dither in the same way as it follows a cavity sweep. The signal from the transmission detector is then demodulated at this dither frequency, after which, it is filtered and recorded on a digital oscilloscope as before.

The main advantage of this dithered cavity sensor is that the cavity dither encodes the absorption information onto the light at a frequency above the region of large technical noise, increasing the resulting signal-to-noise of the sensor. Demodulation of the signal seen at detector D2 at this cavity modulation frequency then decodes the information, and derivative-like absorption features can be obtained. Another advantage is that this technique is sensitive to spectral features of a specific width, and hence the modulation depth can be adjusted to target certain features.

The disadvantage of this sensor is a slight increase in complexity. The modulation technique requires a source, the piezoelectric behavior needs to be understood, and the sensor needs to be more carefully optimized. However, these disadvantages are relatively minor in comparison to the benefits of this sensor.

The next step in the development of cavity-enhanced sensors was to use the technique of resonant sideband detection, or NICE-OHMS (Ye, Ma, and Hall 1998; Gianfrani, Fox, and Hollberg 1999; Ishibashi and Sasada 1999). Figure 1.3 shows the NICE-OHMS experimental arrangement. In addition to the modulation required for the locking of the QCL to the optical cavity, a modulation is applied at the cavity free spectral range (FSR – the frequency interval between consecutive cavity modes), which was 387.5 MHz for these experiments. The resulting sidebands present on the incident field coincide exactly with separate optical cavity modes and thus enter the optical cavity. The field transmitted from the cavity is detected and demodulated first at the FSR frequency, and then at the cavity-dither modulation frequency, these processes being represented by DEMOD1 and DEMOD2 respectively. The resulting signal is then filtered at some bandwidth and monitored during cavity scans as before.

The NICE-OHMS sensor configuration shown here potentially has the best performance of all the presented techniques. To begin with, the resonant sideband technique gives immunity to noise in the lock between the QCL and the optical cavity, becoming more important if cavities with very high finesse are used, which are harder to lock a laser to. The high frequency modulation required to achieve NICE-OHMS results in the FM detection occurring at a frequency where the technical noise on the laser is virtually non-existent, giving the best possible immunity to $1/f$ noise. The cavity-dither technique also employed here allows the selectivity of the instrument to be increased as previously discussed. The result is an instrument with highly optimized sensitivity and selectivity.

While this technique promises a lot, it is considerably more complex. It requires careful matching between cavity length and modulation frequency, which, while not being so extreme as to require an automated system, can be a problem at first (or any subsequent recalibration), because no signal is seen until the matching is reasonably close. Also, the detectors available at these wavelengths do not perform well at high frequencies resulting in considerable loss of signal, and the modulation characteristics of QCLs at these frequencies have not been found to be uniform.

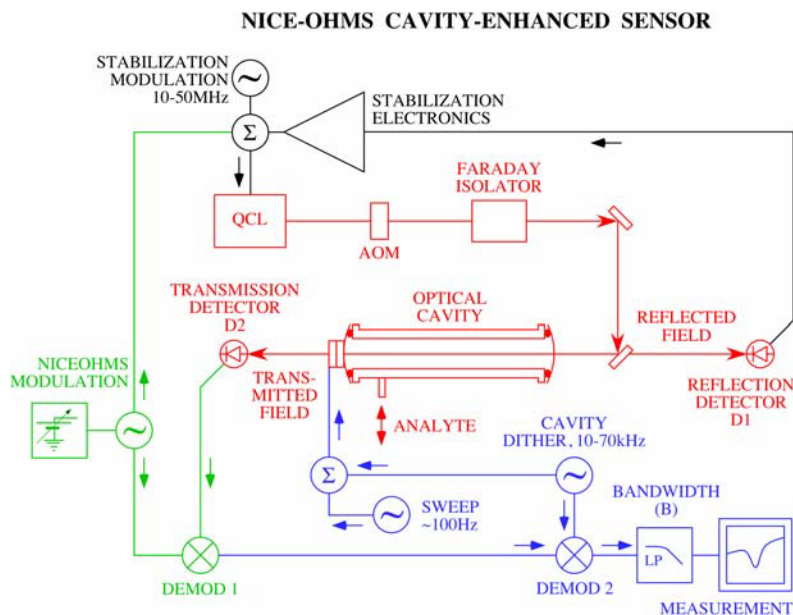


Figure 1.3. NICE-OHMS Recovery Sensor. A high frequency modulation is imposed on the laser in addition to that required for the cavity locking. This high frequency is equal to the spacing between adjacent cavity modes. The resulting transmission signal is first demodulated at this frequency, then secondly at the cavity modulation frequency as explained for the FM recovery cavity-enhanced sensor.

1.2 Achievements in FY03 in Light of FY02 Goals

At the conclusion of the FY02 LWIR CES report, a number of tasks were identified as further work for FY03. This section of the FY02 report is included in the current report as Appendix A. These tasks fall into three broad groups, which we discuss in detail.

1.2.1 Construction of Better Optical Cavities

The finesse of the optical cavities used in FY02 reached a value of 2415. In FY03, cavity finesse values reached 17000, an increase of over a factor of seven, resulting in an increase in potential sensitivity of the cavity-enhanced instruments of the same amount. Other improvements to the optical cavity design included acoustic damping and isolation using specialized sound-absorbing composite materials, and the use of better piezoelectric actuators to improve the dither modulation performance.

1.2.2 Implementation of Amplitude Stabilization to Reduce Optical Fringing Effects

One of the major limitations to the ultimate sensitivity of the simpler cavity-enhanced chemical sensors studies in FY02 is optical fringing. It was envisioned that amplitude stabilization would be able to reduce the effects of optical fringing occurring due to interferometric effects from any optical

components prior to the optical cavity. While this still may well be true, it was found early in FY03 that by far the largest contribution to the optical fringing was occurring due to the interference between the output cavity mirror and the transmission detector, against which the amplitude stabilization is powerless. Consequently, amplitude stabilization was not implemented at this time. It was found later, that using a larger surface area detector greatly reduced the fringing problem. This is discussed in detail in Section 3.4.

1.2.3 Exploring the Limitations of Increasing Cavity Finesse

Practical limitations on the performance of the sensors under development at PNNL will be reached as the cavity finesse is increased. Two ways in which this can happen (outlined in FY02 report) include the possible necessity of an additional servo control loop to fine-tune the NICE-OHMS modulation frequency as the cavity linewidth becomes narrower, and the possible disruption of the cavity mode due to the movement of the dithered cavity transmission mirror. The impact of these issues is discussed below, and explained in some detail in Appendices A and B. While these issues were not found to limit our efforts to increase sensor performance, the issue of saturation proved to be the major limitation when using sub-Doppler features. Considerable attention is given to this in this report, Section 2.

The increase of cavity finesse from 2415 to 17000 causes the NICE-OHMS sensor configuration to be on the verge of requiring active frequency tuning. The higher finesse gave our optical cavity a linewidth of 22.8 kHz. The current cavity tuning range of 1.5 GHz gives a linear change in the FSR frequency of 16.5 kHz, being a significant fraction of the cavity linewidth. For a deployed sensor using this technique with similar cavity specifications, this is clearly an issue. However, for observing a sub-Doppler features requiring cavity scans of a few megahertz, which is our current mode of operation, this is not a problem.

There was no evidence of the second limitation discussed above, that of mode disruption. The cavity dither applied to our sensors currently has a depth equivalent to that of the sub-Doppler features, i.e., around a Megahertz or so. For these depths and a dither frequency of around 60 kHz, there was no evidence of instability in the cavity lock with the increased finesse value of 17000, on or off molecular resonance. Calculating our proximity to this limit requires knowledge of the speed of the dithered mirror. It is not practical to calculate this value as we operate at a resonance of the piezoelectric actuator, which is difficult to characterize. Measuring this value would require dismantling the cavity and assembling a Michelson or equivalent interferometer using the cavity mirrors. This has not been done at this stage because of the disruption to this and other experiments being performed in the laboratory. However, it is strongly suspected that mode disruption will become an issue as we increase the dither depth (and hence the mirror speed) in order to effectively probe Doppler-limited features with our sensors. Work in this area will continue on FY04.

1.3 Progress Independent of FY02 Goals

Our understanding of the interaction of molecular absorption and optical cavities was greatly enhanced over the last fiscal year. Several limitations have been discovered pertaining to the use cavity-enhanced techniques and of high frequency modulation and detection, which specifically limit the applicability of the NICE-OHMS technique to developing a fieldable sensor in the LWIR at this time.

These limitations summarized below, are not so severe as to justify halting research into this technique, but are sufficiently many and varied to require a change of tack if we are to produce a fieldable sensor in a few years. For this reason, it is recommended that our research diversify at this point, allowing the NICE-OHMS technique and that of sub-Doppler FM recovery to remain active research topics, while the techniques of direct cavity transmission detection and Doppler-limited FM recovery become the choices for a fieldable sensor.

The first and most profound limitation is that of saturation. If molecular transitions are pumped hard enough that the excitation rate is faster than the thermalization rates via collisions, spontaneous emission and other processes, the upper levels become significantly populated. This causes stimulated emission to compete with the absorption process, and the medium begins to become transparent. As cavity finesse is increased in order to improve sensitivity, intra-cavity power easily becomes high enough to saturate typical LWIR small-molecule analytes. The resulting reduction in absorption clearly limits the effective sensitivity of the instrument.

The second limitation, which in fact compounds the first, is that we are heavily detector noise-limited. In other words, the dominant noise source is the detection process. This is especially true at high detection frequencies where the responsivity of the mercury-cadmium-telluride (MCT) detectors we use roll off to 35 dB less than the typical DC values. This drastically reduces the possible signal-to-noise ratios using the NICE-OHMS technique, and renders it approximately equivalent in sensitivity to our other best techniques. In addition, this also implies that we cannot reduce the impact of the saturation issue described above by reducing the power circulating in the cavity, as any gains in absorption sensitivity would be wiped out by decreasing signal-to-noise at the detector.

The third limitation involves logistics and the modulation characteristics of the QCL. The NICE-OHMS technique requires the period of the RF modulation frequency to match the round-trip time of the optical cavity, which would require an optical cavity longer than 1.5 m to match a modulation frequency of less than 100 MHz. The requirement for logistically tolerable cavity lengths forces the use of modulation frequencies greater than 100 MHz. In the frequency range above 100 MHz, the QCL frequency modulation characteristics are poor and vary significantly from device to device. In this frequency range, adequate frequency modulation for NICE-OHMS is only possible at a peak in the FM characteristics. Use of a cavity that was too long by 0.5 cm out of a 39 cm cavity length and the required change in modulation frequency made a difference in signal-to-noise ratio of 10 or more. It has already been demonstrated that the optimal modulation frequency is different from laser to laser. This clearly makes building a sensor based on this technique difficult. External modulation techniques have already been demonstrated impractical as the resulting devices finish by being larger and more power hungry than the others that we are already trying to miniaturize for the purposes of making fieldable equipment.

A promising approach that mitigates these problems is to use additional mirrors in the cavity to fold a much longer optical path of the cavity into a package that is the same length as our existing cavity. This approach would decrease the FSR of the cavity and so eliminate the need to modulate the QCL at frequencies above 100 MHz, which is also a frequency region where the responsivity of our MCT detectors is much higher than at 387.5 MHz used for current NICE-OHMS experiments. The additional losses from the increased number of reflections per round-trip in the cavity will reduce the cavity finesse,

but the concomitant increase in cavity optical path length will largely offset the decrease in finesse resulting in approximately the same potential sensitivity. There are two obvious issues with this approach: 1) the increased alignment sensitivity due to the longer length and 2) the polarization changes due to mirror reflections at other than normal incidence. The alignment sensitivity does not appear to be a major issue since the optical pathlength would be similar to that used in many lasers such as large frame argon ion lasers and mode-locked lasers. By keeping the incident angles small and arranging pairs of mirrors so that the polarization changes cancel, it should be possible to solve this issue as well.

2.0 Saturation

Increasing the finesse of the optical cavities in our experiments during FY03 allowed us to see the phenomenon of saturation to be a major limitation when observing sub-Doppler features (Lamb dips) in the LWIR. For this reason, it has been concluded that Doppler-limited spectroscopy be the basis for the development of a fieldable prototype LWIR CES, beginning in FY04. This decision was not made lightly, because the use of sub-Doppler features offered several advantages. The most important of these is that their narrow widths promised much increased selectivity. Overlapping Doppler-limited spectra from different analytes could in theory, be resolved using Lamb dips. The additional sensitivity of Lamb dips to intra-cavity power for a given transition strength could also have added another dimension to the analysis, allowing chemicals to be cross-referenced using saturation strength. Because of these advantages, a careful study was conducted in order to ascertain whether the saturation behavior we were observing could be used or at least backed out of the measurements. Unfortunately, the answer was negative. This study is detailed in this section.

2.1 The Impact of Saturation

The effect of saturation is to render the analyte semi-transparent and thus decrease its absorption of the laser field, and hence, the effective sensitivity of a sensor detecting the saturated medium. In order to see sub-Doppler features, the operating pressure must be low to minimize collisional broadening and hence the washing out of these features. This results in longer lifetimes of excited states, which are thus more easily populated and saturated. In the latest round of experiments using a cavity finesse of 17000, saturation parameter values (see Section 2.2 for definition) of over 60 were observed in nitrous oxide for normal operating powers. Moreover, the observed transitions in this gas in this region are vibrational overtones or combination bands that are forbidden in the harmonic oscillator approximation, and hence are actually weaker than could be otherwise observed in similar gaseous species. It is estimated that for comparable fundamental transitions, saturations of 600 to 10,000 might be expected, with a corresponding decrease in effective instrument sensitivity of up to a factor of 100 in comparison to what would be observed in the absence of saturation. This reduction in sensitivity is not the only issue. It is power-dependent and different for different species. This makes chemometric comparisons between gases very difficult.

The connection between transition saturation and cavity finesse is intra-cavity power. One way to increase the sensitivity of the sensors under study is to increase the cavity finesse. This happens when the mirror reflectances more closely approach unity, and the intra-cavity losses, zero. The results of increased finesse are narrower cavity linewidth, higher intra-cavity (circulating) power for the same input-coupled power, and higher sensitivity to optical losses, such as the presence of an absorbing medium. This latter point can be thought of, in the limit of small absorption, as increasing the effective absorption path length. The increased intra-cavity power and the low pressure LWIR analytes inside the cavity result in higher saturation values. The immediate thought is to reduce the input power, and avoid this issue. However, this results in reduced transmitted power, which can never be more than the incident power. To make matters worse, in high finesse cavities, the transmitted power is often considerably less than the

input-coupled power because mirror coatings losses are often comparable to transmission values. Consequently, increasing the cavity finesse in a manner that attempts to maintain constant intra-cavity power will nearly always result in a more than commensurate loss in transmitted power. The resulting decrease in signal-to-noise of the detector is something we cannot afford, since we are already detector noise-limited.

The effects of saturation in a given sample can be reduced by adding a buffer gas and increasing the pressure. This decreases the excited state lifetimes via collisional de-excitation, thus decreasing the upper state populations and saturation levels. Collisions also cause dephasing, which broadens the homogeneous linewidth and so decreases the interaction between the analyte and the optical field, further decreasing saturation. The broadening that occurs due to these processes washes out the sub-Doppler features, meaning that the sensor would have to rely instead on Doppler-limited spectroscopy. The resulting spectral features will be broader, but they will not saturate readily, and hence the absorption values won't be reduced by saturation effects. Their ratios should not be power- and thus sweep-dependent and should therefore allow chemometric fitting to be more readily performed.

Increasing buffer gas pressure to decrease saturation begins to reduce selectivity and absolute sensitivity when the pressure broadened homogenous width matches the inhomogeneous linewidth. For an analyte in the LWIR that has resolved Doppler broadened transitions, this occurs at a buffer gas pressure of about 5 Torr. Vibrational transitions in large molecules with unresolved rotational structure can tolerate even higher buffer gas pressures before selectivity is reduced.

Vibrational transitions in the LWIR saturate more readily than those in the visible and NIR because of their greater strength. Nevertheless, we were surprised at the low intensities required to saturate the nitrous oxide transitions we observed.

2.2 The Nature of Saturation

Saturation depends only on the transition dipole moment, the laser intensity and the interaction time. If these values are held constant, its effect is not reduced by lowering the analyte pressure, or even choosing lines of smaller absorption cross-section. (The reason why pressure broadening can reduce saturation is that it affects the interaction time as explained earlier.) After this realization, a modeling study was undertaken to ascertain the effects of saturation on intra-cavity absorption features in the low-pressure limit where pressure broadening is small. Effects on both the Doppler profiles and sub-Doppler features are considered. The widths and depths of these features, and the required absorption conditions for the optimization of sub-Doppler features such as Lamb dips, were modeled in detail. Various trends were identified in the behavior of these features in an attempt to find a way to allow all the absorption information to be extracted from a saturated sub-Doppler profile. However, it has become clear that it would very difficult to differentiate between absorption signatures of saturated molecular transitions and those of stronger but unsaturated transitions of equivalent absorption strength. This in turn makes it difficult to determine either the saturation or unsaturated absorption coefficients of a given set of features. This makes it difficult to positively identify the concentrations of gaseous compounds in a given mixture unless saturation is negligible or well known.

2.3 The Effects of Saturation on Strength and Depth of Absorption Features

Due to saturation, the peak absorption strength of homogeneous features is reduced by the saturation of the medium by the factor (Demtröder 1996, p. 253),

$$\frac{1}{1 + \frac{I}{I_{sat}}} = \frac{1}{1 + S_0}$$

where I_{sat} is the saturation intensity at which the Rabi frequency equals the homogeneous linewidth, and S_0 is the peak saturation parameter, defined as,

$$\begin{aligned} S_0 &= \left[\frac{\mu_{12} E_0}{\hbar} \right]^2 \cdot T_1 T_2 \\ &= \left(\frac{\mu_{12}}{\hbar} \right)^2 \cdot \frac{2}{c \epsilon_0} \cdot I_0 T_1 T_2 \end{aligned}$$

where μ_{12} is the transition dipole moment in Coulomb-meters (but usually quoted in Debye), E_0 is the electric field amplitude, I_0 is the optical intensity and T_1 and T_2 are the population and coherence decay times of the transition. (In the case of transit-time broadened transitions, we can set $T_1 = T_2 = T_u$.) At frequencies other than zero detuning from the center of the absorption feature, the saturation parameter varies similarly to the absorption,

$$S(\omega) = S_0 L(\omega)$$

where $L(\omega)$ is the unit-height line shape function, typically Lorentzian for homogeneous features. The homogeneous saturated absorption coefficient is then,

$$\alpha_{sh}(\omega) = \frac{\alpha(\omega)}{1 + S(\omega)}$$

where $\alpha(\omega) = \alpha(\omega_0) L(\omega)$, ω_0 being the zero detuning frequency of the homogeneous absorption feature. After some inspection, it is clear that the preferential reduction of stronger regions of the absorption feature also results in a broadening of the homogeneous linewidth $\delta\omega_h$, which can easily be shown to be

$$\delta\omega_{sh} = \sqrt{1 + S_0} \cdot \delta\omega_h$$

Figure 2.1 shows the profiles of various functions for peak saturations of 1.0 and 0.3. (Dfwhm and Lfwhm are Doppler and Lorentzian full-width half-maximum, respectively.)

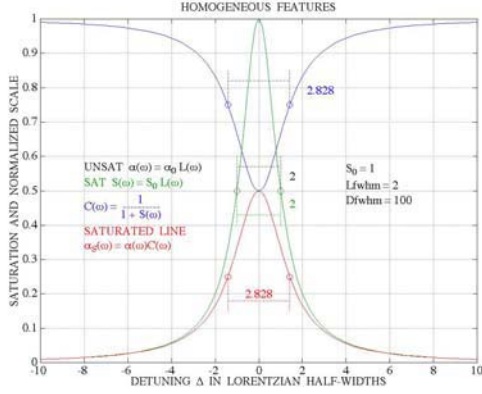


Figure 2.1a. Absorption and Saturation Functions for Peak Saturation Parameter of 1.0

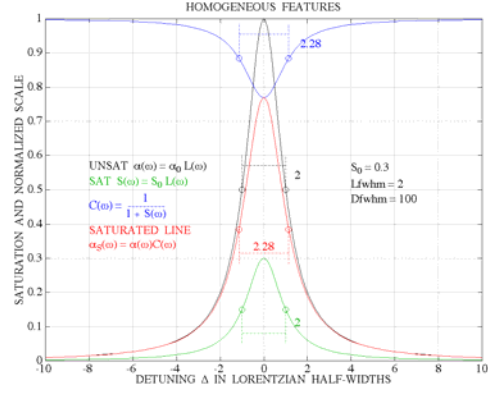


Figure 2.1b. Absorption and Saturation Functions for Peak Saturation Parameter of 0.3

On the other hand, inhomogeneous features, such as Doppler-broadened profiles, always have a subset of molecules whose homogeneous center frequency matches the laser frequency if the laser is within the inhomogeneous profile. The resulting absorption strength is,

$$\begin{aligned}\alpha_{si}(\omega) &= \frac{\alpha^0(\omega)}{\sqrt{1 + S_0}} \\ &= \frac{\alpha_0 D(\omega)}{\sqrt{1 + S_0}}\end{aligned}$$

where $\alpha^0(\omega)$ is the unsaturated inhomogeneous profile, α_0 is the peak inhomogeneous absorption and $D(\omega)$ is the unit-height inhomogeneous line shape, typically being Gaussian due to Doppler-broadening. Because of the appearance of S_0 rather than $S(\omega)$ in this expression, it is evident that inhomogeneously broadened features are not affected in width by saturation, provided that the underlying saturated homogeneous width is much smaller than the inhomogeneous width. As we shall see, the addition of an optical cavity can modify these statements.

2.4 The Effect of Saturation on Homogeneously Broadened Intra-Cavity Absorption Features

It must be understood, that saturation and absorption are two different phenomena. To say a transition is saturated means that the interaction between the light and the molecules is strong enough to sufficiently populate the upper level of the transition as to reduce the amount of absorption from the optical field. This does not imply however, that the amount of absorption need be particularly large for this to occur.

If the optical field is significantly affected by the absorption due to a saturated medium, it is then clear that the saturation parameter is in turn affected by the intensity change of the optical field. This happens inside an optical cavity when the single path absorption is comparable to the mirror transmission. The normalized circulating intensity inside an optical cavity containing a saturated inhomogeneously-broadened medium, can be written

$$\frac{I_c(\omega)}{I_{c0}} = \frac{1}{\left[1 + \frac{F_E L \alpha_{si}(\omega)}{\pi}\right]^2}$$

where I_c is the intra-cavity intensity of peak value I_{c0} , F_E is the finesse of the empty cavity of length L . Since both the transmitted cavity intensity I_t and the intra-cavity saturation parameter S_c are directly proportional to I_c , we see that their normalized forms are equal, and can be written

$$\begin{aligned} p &= \frac{I_c}{I_{c0}} = \frac{I_t}{I_{t0}} = \frac{S_c}{S_{c0}} \\ &= \frac{1}{\left[1 + \frac{F_E L \alpha_{si}}{\pi}\right]^2} \end{aligned}$$

where explicit frequency dependence has been dropped. Inside the optical cavity, the saturated absorption strength is now

$$\alpha_{si} = \frac{\alpha^0(\omega)}{\sqrt{1 + S_c}}$$

Notice that S_c is a function of detuning in this case because of the changing cavity intensity, specifically, $S_c = p \cdot S_{c0}$. Solving these two equations leads to a quartic polynomial, which when solved numerically, shows a narrowing of the saturated profile compared to an unsaturated profile of equivalent absorption strength. Note that both are broadened by the action of the cavity compared to the non cavity-enhanced case, simply because the impact of absorption is increased by the action of the optical cavity, flattening of the top of the feature. Figure 2.2 shows an example of this.

The amount of narrowing that occurs is a function of the empty cavity saturation parameter, and the absorption strength. A 3-D plot of this function is shown in Figure 2.3a as well as the corresponding plot of minimum normalized cavity intensity $p(\omega)$ in Figure 2.3b. We can see that the narrowing appears to be a strong function of saturation up to the peak value after which it gently returns, and its dependence on absorption factor ($\alpha_0 F_E L / \pi$) is approximately logarithmic for saturation values of interest below the peak. This latter point makes it particularly difficult to fit data to the theoretical surface. Moreover, the

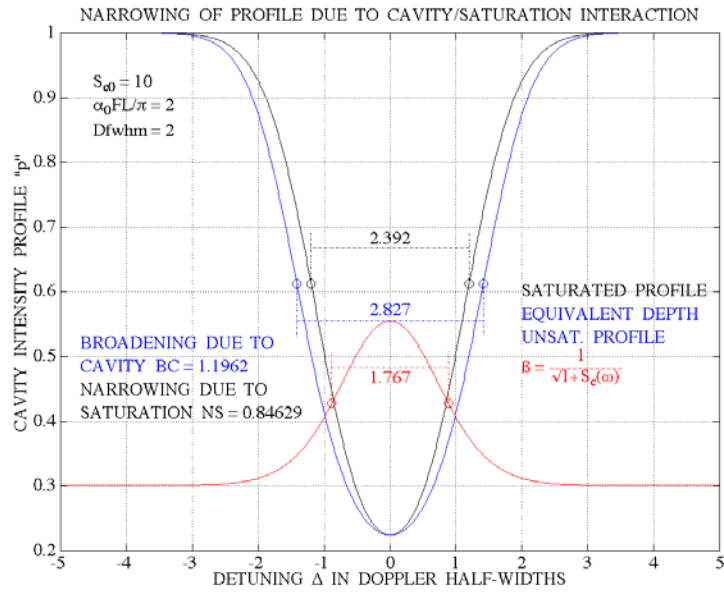


Figure 2.2. Narrowing Due to Saturation as Compared to an Unsaturated Profile of Equivalent Depth is Shown. Note that both features are broadened simply by the interaction between analyte and optical cavity.

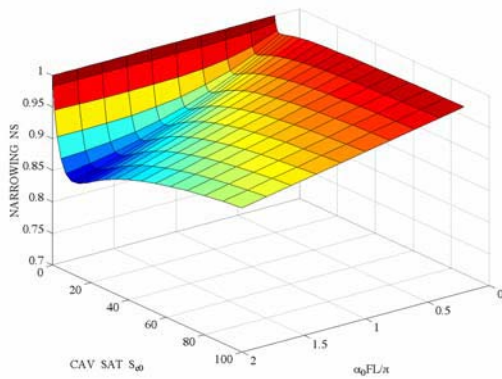


Figure 2.3a. 3-D Plot of the Narrowing of the Saturated Intra-Cavity Doppler Feature as Compared to the Width of an Unsaturated Feature of Equivalent Depth

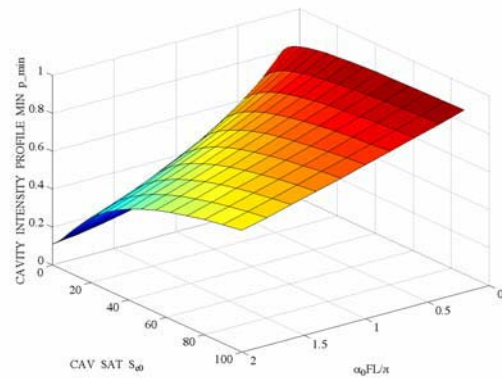


Figure 2.3b. 3-D Plot of the Cavity Intensity Function p vs. Absorption Factor and Empty Cavity Saturation

function is not particularly deep. The case shown in Figure 2.2 is for the extreme values in Figure 2.3 – an empty cavity saturation value of 10 and an absorption factor of 2 yielding a narrowing of only about 0.85. Given the nonlinearity of cavity piezoelectrics and QCL sweeps this would be easy to miss

experimentally. It is thus not at all obvious how one could use this narrowing to distinguish between a saturated transition and an unsaturated one of equivalent absorption strength.

2.5 Sub-Doppler Absorption Features and the Lamb Dip

Beginning again with the unsaturated Doppler-broadened profile of $\alpha^0(\omega)$, the intra-cavity standing wave line shape is found to be $\alpha_L(\omega) = \alpha^0(\omega) \cdot M(\omega)$ where $M(\omega)$ could be called the Lamb dip generator function, and is found to be (Demtröder 1996, p. 443)

$$M(\omega) = \frac{\delta\omega_h/2}{B\sqrt{1 - \left(\frac{2\Delta}{A+B}\right)^2}}$$

$$A(\omega) = \sqrt{\Delta^2 + \left(\frac{\delta\omega_h}{2}\right)^2}$$

$$B(\omega) = \sqrt{\Delta^2 + \left(\frac{\delta\omega_h}{2}\right)^2} \cdot (1 + 2S_0)$$

where $\Delta = \omega - \omega_0$ is the detuning. One finds after some algebra that the value on line center and just off line center (but still within the inhomogeneous linewidth) respectively are

$$M_{\Delta=0} = \frac{1}{\sqrt{1 + 2S_0}}$$

$$M_{\Delta \gg \delta\omega_h} = \frac{1}{\sqrt{1 + S_0}}$$

leading to the well-known expression for maximum theoretical Lamb dip depth

$$\Delta M = \frac{1}{\sqrt{1 + S_0}} - \frac{1}{\sqrt{1 + 2S_0}}$$

having a maximum value of 13% at $S_0 = 1.4$. Lamb dips for various values of saturation are shown in Figure 2.4. It is important to note that the 13% is relative not to the saturated inhomogeneous absorption profile, but to the unsaturated value. The value relative to what the size of the actual saturated profile would be in the absence of a Lamb dip approaches a value of around 30% with increasing saturation. The width of the Lamb dip in the generator function itself is very slightly larger than that of a saturated homogeneous feature (typically 1.05), but some reduction and increased variation in the actual Lamb dip width is caused by the additional effect of the shape of the Doppler background. At optimum values, the Lamb dip width is about 0.96 of that of a saturated homogeneous feature.

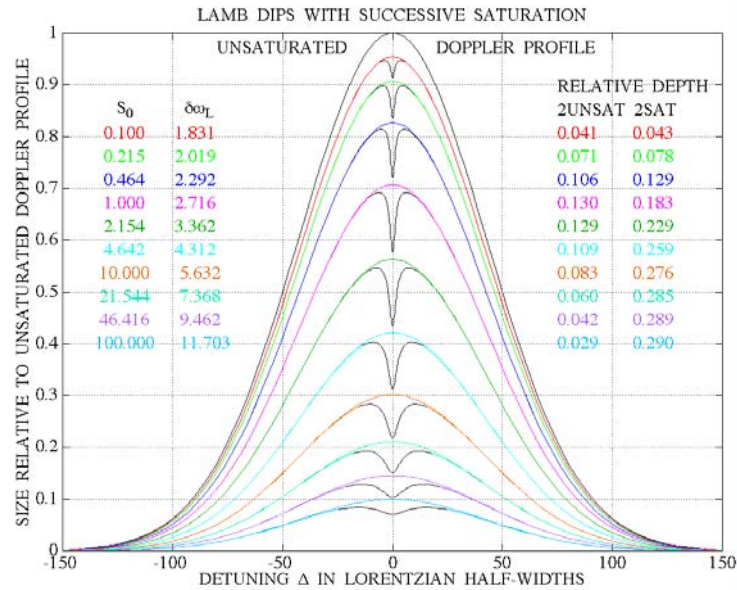


Figure 2.4. Lamb Dips for Absorption Profiles with Various Saturation Levels. The maximum size Lamb dip is about 13% of the size of the unsaturated inhomogeneous feature and occurs when the saturation parameter is about 1.4. The relative size of the Lamb dip with respect to the saturated inhomogeneous feature however asymptotes to about 30% as saturation increases.

2.6 Effect of Saturation on Sub-Doppler Intra-Cavity Absorption Features

As could be expected from preceding sections, the action of an optical cavity modifies the behavior of the Lamb dips. In order to quantify these effects, the Lamb dip generator equation must be solved in conjunction with the cavity intensity equation. This is an intractable analytical problem, but is easily solved on a computer using simple iterative techniques. Using the completely inhomogeneous case as a starting point, the Lamb dip can be added to first order by ignoring the resulting change in cavity intensity, then, iterative corrections can be made to include the impact of the Lamb dip on the intra-cavity field. The iteration is found to converge rapidly after eight iterations to give a result within 0.1% tolerance. Figure 2.5 shows the intra-cavity Lamb dip with the same parameters used in Figure 2.2. Again the equivalent depth unsaturated profile is shown for comparison. It can be seen then that the result of the cavity interaction in the presence of significant absorption is to deepen and slightly broaden the Lamb dip, whereas the effect on the inhomogeneous background was a slight narrowing compared to the unsaturated profile of equivalent depth.

A sequence of intra-cavity Lamb dips solved in the same fashion is shown in Figure 2.6, this time for an absorption factor of unity. As can be seen, the size of the Lamb dip relative to the unsaturated inhomogeneous profile continues to have a maximum value of around 13%, but the empty cavity saturation value for which this occurs is much higher because of the cavity interaction with significant

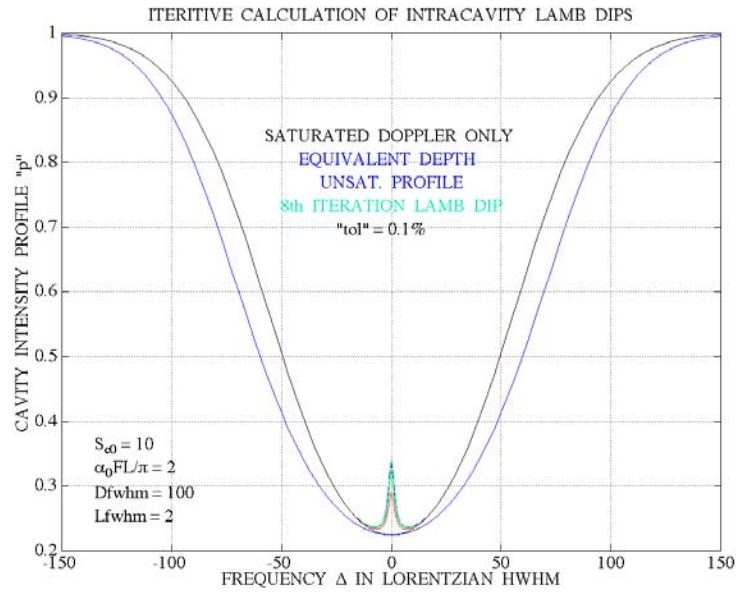


Figure 2.5. Iterative Solution of Intra-Cavity Lamb Dip Problem. The solution converges to within 0.1% after eight iterations. The effect is to deepen and slightly broaden the Lamb dip.

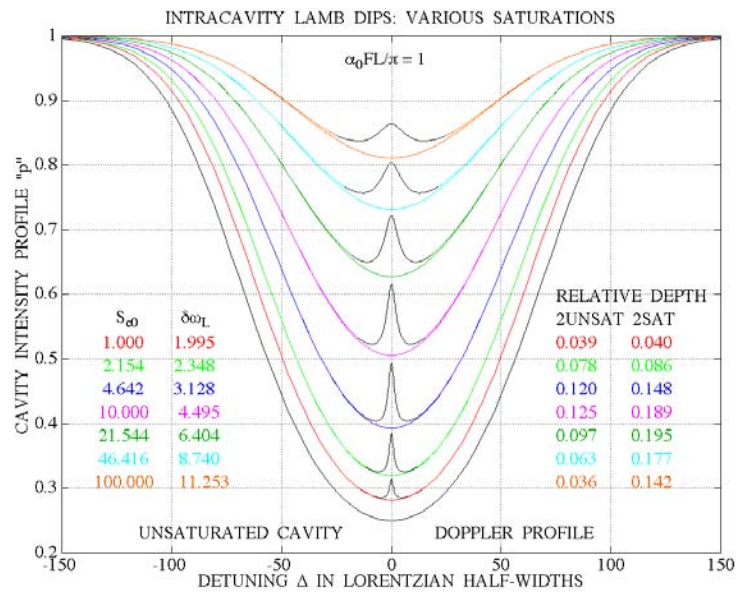


Figure 2.6. A sequence of intra-cavity Lamb dips solved using the iterative technique described above. The maximum Lamb dip size relative to the unsaturated inhomogeneous feature is still roughly 13%, but this time occurs at an empty cavity saturation value considerably higher for significant intra-cavity absorption.

absorption. The saturation occurring at the peak of the feature is still the same as the original calculations, but this corresponds to a much larger empty cavity saturation value, and the latter quantity is much easier to work with experimentally. Also, note that the Lamb dip size relative to the saturated inhomogeneous feature also has a distinct maximum this time, which peaks somewhat later than that relative to the unsaturated value. This is brought out more in Figure 2.7. Note that the empty cavity saturation values required to achieve peak Lamb dip sizes become significantly larger as the absorption factor is increased – the saturation axis is logarithmic!

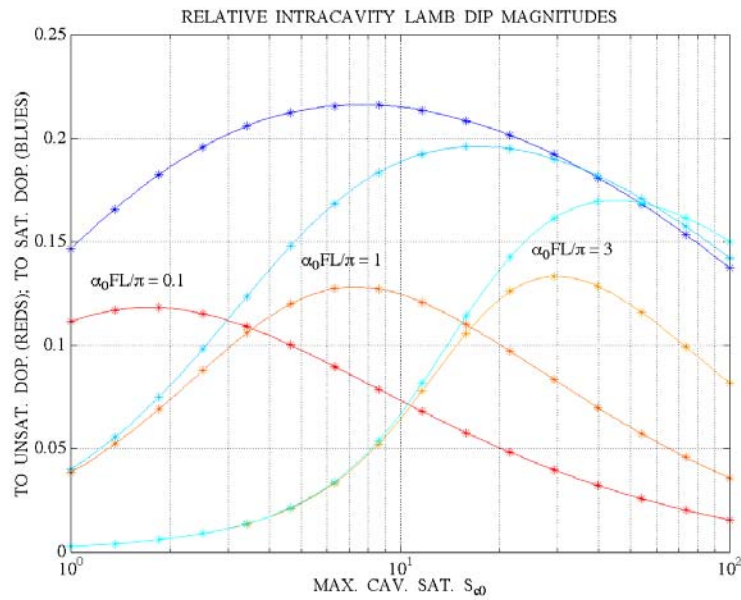


Figure 2.7. Lamb Dip Size Relative to Unsaturated Inhomogeneous Feature (red/orange traces) and Relative to Saturated Features (blue/cyan traces). As the absorption factor increases, the maximum size Lamb dip occurs for significantly larger empty cavity saturations. The value of the absolute maximum gently increases with increasing absorption, whereas the maximum relative size decreases.

The salient feature here is that the change in absolute Lamb dip size is relatively small with changing saturation, which again makes uniquely fitting the model to data difficult – a given Lamb dip size will not give a significant indication of how saturated the transition might be.

Finally the effect of saturation on the Lamb dip width is to be considered. Figure 2.8 shows this effect. Again, we see no great difference in the behavior of the Lamb dip width for different values of absorption factor, the greatest difference occurring for empty cavity saturation values around 10, the difference being by a factor of about 2.5.

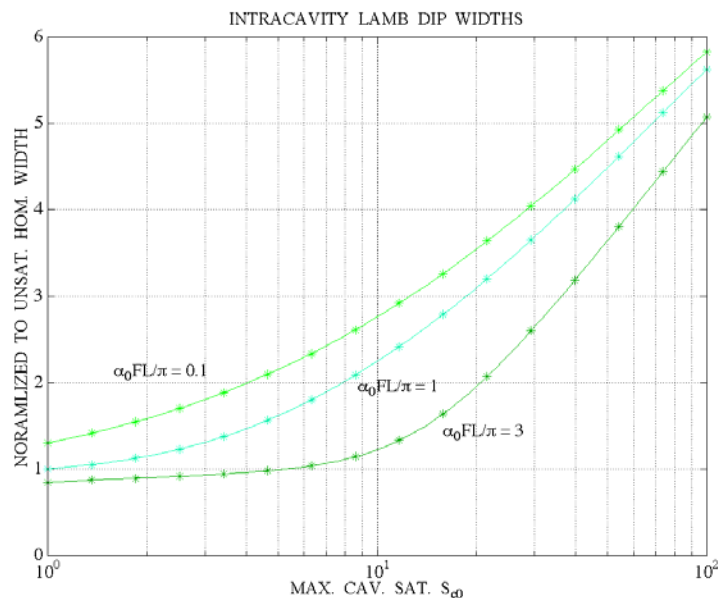


Figure 2.8. Lamb Dip Width as a Function of Empty Cavity Saturation for Various Absorption Factors

Conversely, one could say for example, that for a given Lamb dip width of twice the homogeneous width, the absorption factor could be anything from 0.1 to 3.0 corresponding to saturation values anywhere from 4 to 20. Therefore, a given Lamb dip width doesn't pin down absorption or saturation.

2.7 Conclusions about the Impact of Saturation on Sensor Performance

Saturation is an issue that could prevent cavity-enhanced techniques reaching their advertised sensitivities at low pressures in the LWIR. This would compromise the performance of sensors based on sub-Doppler features such as Lamb dips. While it may be possible to use the effects of saturation on the width and depth of both the inhomogeneous and sub-Doppler lineshapes, to positively determine both the saturation and the absorption coefficient of a given medium, it is not clear from inspection how to do so. It is equally unclear that once discovered whether such a method would be useful, practical or accurate.

It is recommended as suggested in the summary introduction, that a study be undertaken into the transition dipole moments of specific molecules of study. This study could then be extended to more complex analytes such as simulants of explosives etc. The latter represents a significant undertaking because little is known about the transition dipole moments of some of these compounds. It is however fairly easy to experimentally determine the saturation intensities of various analytes using the LWIR cavity-enhanced sensors already developed at PNNL. By comparing behaviors with direct absorption, then cavity-enhanced absorption using various cavity finesse values, several points can be taken and the saturation value of the compound be estimated. Accordingly, a maximum practical value of cavity finesse can then be chosen for particular analytes to avoid saturation effects for each of these analytes.

3.0 Mercury-Cadmium-Telluride Detectors

3.1 Detectors in the LWIR

Finding high-speed detectors with high quantum efficiency and low noise in the LWIR is much more difficult than in the visible or NIR. Traditionally, mercury-cadmium-telluride (MCT) detectors have been used in the LWIR. The low band gap of these devices results in much higher noise levels both because of the sensitivity to the thermal blackbody background and because of the much higher leakage currents, both with their associated shot-noise currents. The low shunt resistance of MCT detectors also leads to more noise from the associated pre-amps. In theory, the quantum efficiency and frequency response of these devices are not significantly degraded compared to their visible and NIR counterparts, silicon and indium-gallium-arsenide (InGaAs) respectively. In practice, current commercially available MCT detectors do not approach this ideal. The lack of significant commercial applications for sensitive LWIR detectors with bandwidths greater than 100 MHz limits the available detector choices. This situation is exacerbated by the move by much of the commercial sector away from single element IR detectors and towards focal plane arrays and the move by some companies during the telecom boom away from LWIR detectors and towards NIR detectors. While it is possible to find LWIR detectors that are fast, it is proving very difficult to find fast LWIR detectors that are low noise and have good responsivity. Even finding reliable high frequency performance data on these detectors is difficult, as manufacturers will often say that they have no modulated optical source operating at these wavelengths with which to test their detectors. It is our impression that this is not because of any physical or technical limitation, but rather reflects the current state of the market and the availability of suitable optical sources in the LWIR. This situation can only be rectified by working with detector manufacturers to help develop and characterize better detectors, most probably using modulated QCLs or heterodyne beats between matched pairs of QCLs for this purpose. QWIP detectors are another promising alternative to MCTs, but as mentioned above, it seems virtually impossible to purchase single element detectors, and the available QWIP arrays are so far unsuitable for our work.

Since the beginning of our work with QCLs, we have chosen cryogenic photovoltaic MCT detectors for use in our chemical sensor designs, as they exhibit relatively low noise and good responsivity (or alternatively “detectivity D^* ”) at frequencies below 100 MHz compared to other detectors operating at the same optical wavelengths. However, our work with NICE-OHMS has caused us to look more closely at their high frequency performance, which has been found to degrade rapidly with frequency.

The photovoltaic MCT detectors we use operate at cryogenic temperatures, which reduces leakage currents, and are housed in small dewars with a protruding mount for the detector and window, and an electrical connector on the opposite side of the dewar some distance away. Inspection of the internal connections between the connector and detector has shown them to be simple wires, with no consideration given to impedance matching or high frequency signals. While the preamplifiers we constructed to operate with these detectors were designed to be fast, stable and matched to the shunt resistance of the detector to minimize noise, it was not expected that the high frequency characteristics

would be well matched. A recent impedance measurement of one of these MCT detectors is shown in Figure 3.1.

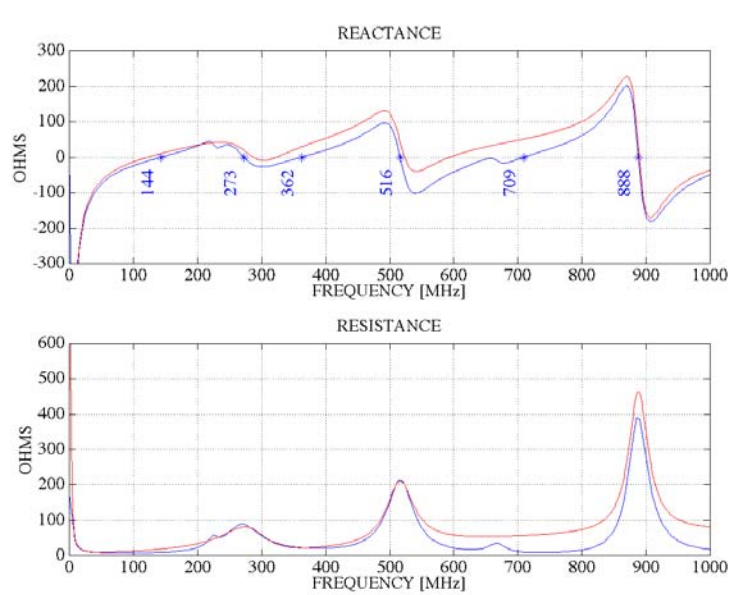


Figure 3.1. Measured Impedance Function (blue) and Modeled Impedance Function (red) of a 100 Micron Diameter MCT Detector. The top panel shows the imaginary, or reactive, part of the impedance, and the bottom panel is the real or resistive part. As evidenced by the discrepancy between the blue and red curves, it is not easy to model all the effects of a lumped-impedance.

The blue curves are the measured impedance, while the red curves are the theoretical impedance of a circuit closely modeling the detector, shown in Figure 3.2. As could be expected from a device with such poor high frequency connections, the imaginary part of the impedance, also known as the reactance, changes sign several times between zero and 1 GHz. The frequencies where the reactance is zero are shown in Figure 3.1 and these zero crossings indicate that the detector is repeatedly changing from appearing capacitive to inductive and back again. This occurs when there are multiple resonances. The regions of high real impedance occurring concurrently with the larger sharper resonances indicate a series of parallel resonances. The more gentle, intervening zero crossings of the imaginary part with little or no accompanying real part indicate series resonances. In the model, these series resonances occur between components in separate blocks of parallel components.

It is more than reasonable to assume that so many resonances would negatively impact the response of the detector-preamplifier combination. In addition, with such a complicated impedance function, trying to compensate for it by constructing a broadband matching circuit is not practical. Recently however, similar cryogenic photovoltaic MCT detectors were purchased that had output connectors mounted directly above the detector elements, which we will refer to as a “close-coupled” detector since it allows close coupling of the detector to the preamplifier. The close-coupled units were advertised as having better high frequency performance.

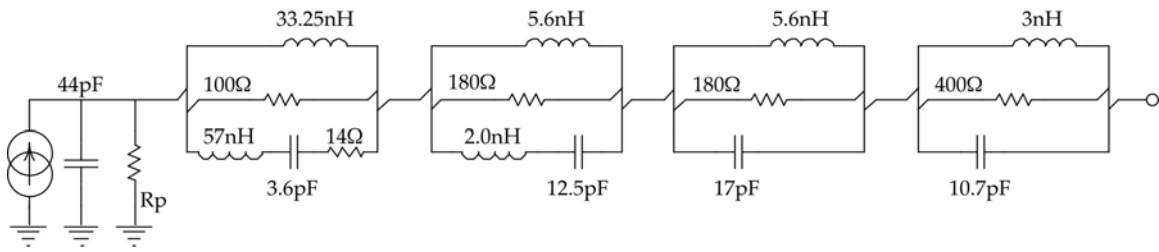


Figure 3.2. Circuit Approximating MCT Detector with Poor High Frequency Connections. The detector has shunt capacitance between anode and cathode in addition to shunt resistance due to leakage. However, the poor high frequency connections between the detector and the connector on the dewar give rise to the various blocks of parallel resonances. Series resonances exist between various components in adjacent blocks.

Figure 3.3 shows the impedance response of one close-coupled detector, again the blue curve showing the measured impedance response and the red showing the theoretical response of a model used to approximate the detector.

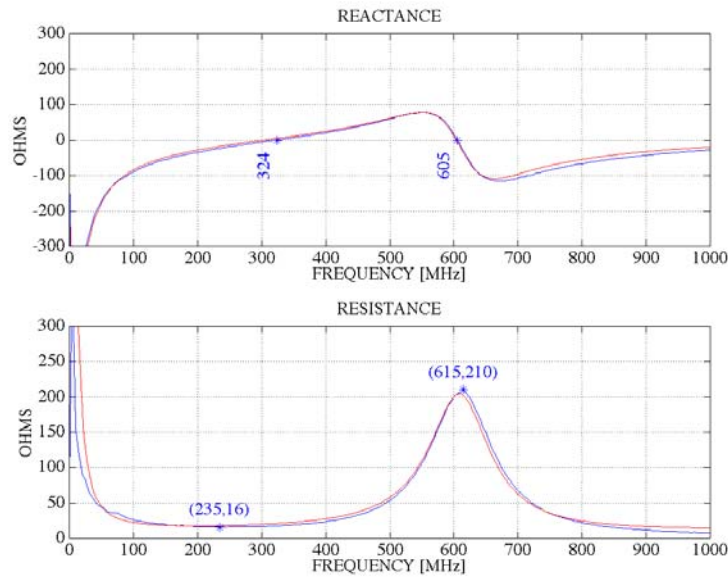


Figure 3.3. Measured Impedance Function (blue) and Modeled Impedance Function (red) of the New 100 Micron Diameter Close-Coupled MCT Detector. Again, the top and bottom panels show the reactive and resistive parts respectively. The response is much less complicated than those shown Figure 3.1, and the matching of the model is much better.

The impedance response is much simpler, as would be expected due to the better high frequency transmission of the close connection to the detector element, with only one series and one parallel resonance at 324 and 605 MHz, respectively. This is confirmed by the relative simplicity of the model shown in Figure 3.4.

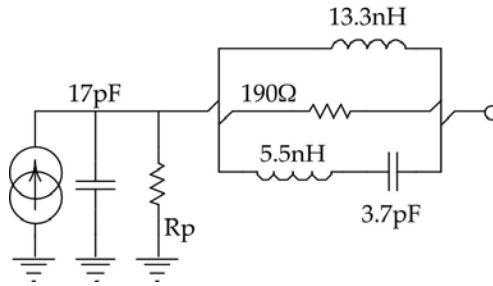


Figure 3.4. Relative Simple Model of the New 100 Micron MCT Detectors with Close Connections. Only one block of parallel resonances as compared to four in Figure 3.2.

3.2 Transfer Function Measurements

It was thought until recently that the poor high frequency response was explainable by poor matching between detector and preamplifier, and also by the complexity of the MCT detector impedance response. However, with the close-coupled MCT detectors with the simpler response, we were able to build the circuit shown in Figure 3.4, and use it to simulate the impedance response of the detector. The response of this circuit was tested on a network analyzer and found to agree with the curves shown in Figure 3.3 out to about 500 MHz. This enabled us to inject a high impedance signal in place of the current source in the model and test the response of the detector-preamplifier combination. The response of this combination was surprisingly good, as shown in Figure 3.5.

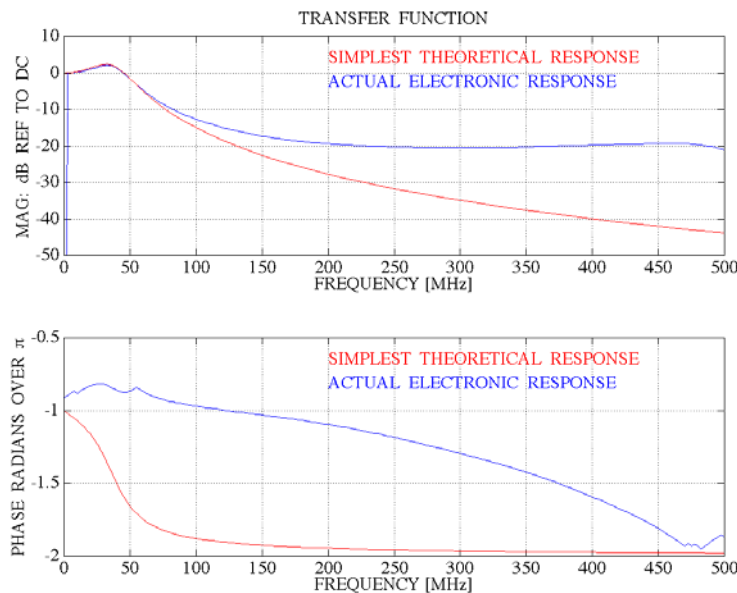


Figure 3.5. Transfer Function Response of Simulated Detector and Preamplifier Combination (blue), as Compared to the Theoretical Response (red) of an Ideal Detector and Transimpedance Amplifier as Shown in Figure 3.6. The top and bottom panels show amplitude and phase response of the transfer function.

The blue curve is the measured transfer function response of the simulated detector and preamplifier combination. The vertical scale is normalized to zero dB at DC. The red curve is the theoretical response of an ideal detector with an ideal transimpedance amplifier as shown in Figure 3.6. This “ideal” response, looks like that of a damped second order resonance, rolling off at 12 dB per octave. The reason why this happens is that the input of the transimpedance amplifier looks like an inductance to the capacitive detector element. The result is a resonance, in our case occurring at around 35 MHz. The feedback capacitor placed across the amplifier in Figure 3.6 acts just like a resistor in the equivalent L-C circuit, damping the peak of the resonance.

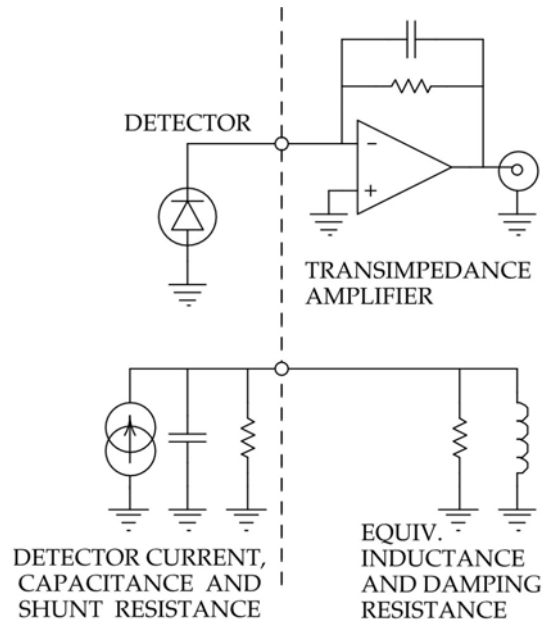


Figure 3.6. Simplest Form of Detector and Transimpedance Preamplifier (top) and the Equivalent Impedance Circuit (bottom). The detector has some capacitance between anode and cathode, and some shunt resistance due to leakage, and the photocurrent produced appears like a current source as drawn in previous cases. However, in this case there is no inductance and no extraneous resonances. The inverting input of the amplifier and feedback resistor combination looks like an inductor forming a simple resonance, while the compensation capacitor has the effect of adding a damping resistor across the inductor in the equivalent circuit.

It is not a fundamental problem that the response of our system is larger than that of the ideal case: it simply means that both our detector and preamplifier are more complicated than the ideal case, and the extra reactance in the circuit and high frequency response of the preamplifier are positively influencing the transfer function.

3.3 Falling Responsivity

Ironically, the simpler impedance of the close-coupled detector and the reduced shunt capacitance did not yield an improvement in detector-preamplifier performance. As shown in Figure 3.5, the measured transimpedance gain (in ohms (Ω)) at 387.5 MHz (the NICE-OHMS modulation frequency) of the close-coupled detector equivalent circuit and preamplifier was found to be 19.2 dB below the DC level of 5.2 k Ω , i.e., 570 Ω . By measuring the noise at the output of the preamp without laser illumination, using this calculated gain, we obtained a dark current noise at the photodetector element of 4.04 pA/ $\sqrt{\text{Hz}}$. Illuminating this detector with laser light producing a photocurrent of 192 μA , (shot noise of 7.85 pA/ $\sqrt{\text{Hz}}$), should increase the noise level by about 6.8 dB. However, only about 0.5 ± 0.2 dB was observed. Reversing the calculation and using the same measured dark noise level yields a transimpedance gain of only $102 \pm 24 \Omega$, corresponding to reduction in gain from the DC level by 34 ± 2 dB, 15 ± 2 dB more than the 19.2 dB predicted from the transfer function. The only possibility for this 15 dB loss in signal is the detector responsivity, i.e., the relationship between the electrical current the detector produces to the optical power incident on it, has fallen.

The detector responsivity is incredibly difficult to measure. The reason is the same one alluded to earlier about which detector manufacturers often complain: one needs a calibrated modulated source to illuminate the detector, and to know the exact response of the preamplifier, which unfortunately depends of the impedance of the detector. Even after fully electrically characterizing a detector as we have done here, we still cannot illuminate it with an amplitude-modulated QCL and back out a detector response from this, because the QCL response is a part of this measurement. Alternatively, one needs a calibrated detector-preamplifier response to measure the QCL response.

There is, however, a way to measure the response of the detector-preamplifier combination without implicitly including the QCL modulation function: use the heterodyne signal obtained by beating two unmodulated QCLs on the detector element. The frequency of the signal on the detector is now simply the detuning between the two lasers, and its amplitude is essentially constant for changes in frequency across the entire detector operating range. The results of just such a measurement performed with both the older style and close-coupled detectors, is shown in Figure 3.7.

The red trace shows the heterodyne response of the older style detector with poorly designed connections between the detector element and output connector. The effects of the resonances are evident, although not in exactly the same places as shown in Figure 3.1, indicating some errors in our modeling process. The blue trace shows the heterodyne response of the close-coupled detector. It is incredibly disappointing the response of the close-coupled detector is lower in magnitude than that of the older unit. It appears that the extra resonances of the more poorly designed detector actually aided in producing a larger response. Attempts were made to utilize this phenomenon to enhance the response of detectors, for example, by adding inductance in the preamplifier input to isolate the amplifier from the detector capacitance, but to no avail. Earlier attempts were made to use active components (transistors) to isolate the detector in a similar way, with similar results: much fewer resonances but lower response. It seems that nothing works better than the non-optimized detector and simple transimpedance preamplifier, despite the accompanying resonances.

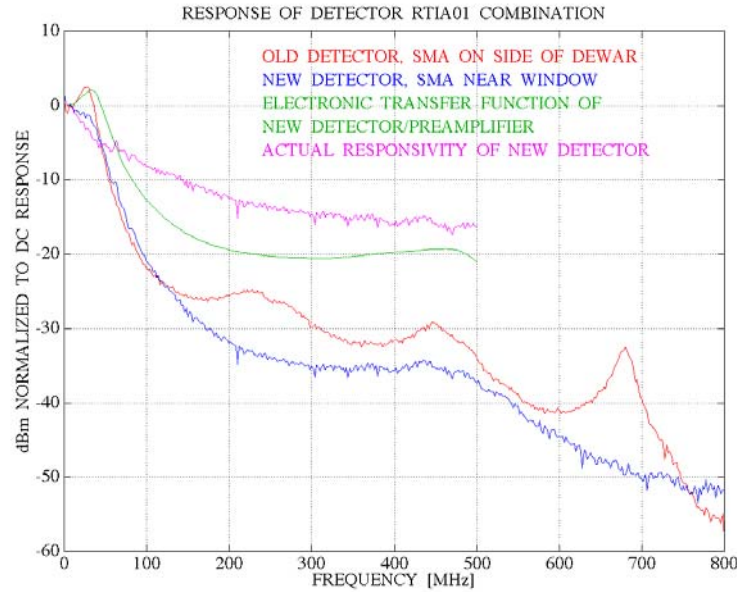


Figure 3.7. Comparison of Heterodyne Measurements of Detector-Preamplifier Response Using Both Old (red) and Close-Coupled (blue) Detectors. Also shown is the measured transfer function shown earlier in Figure 3.5 (green) used to back out the responsivity of the new detector (magenta).

Also shown in green in Figure 3.7, is the transfer function of the simulated close-coupled detector and preamplifier combination measured in Figure 3.5. Dividing the blue curve by this one produces the frequency dependent responsivity of this detector. This curve is now (supposedly) independent of the electrical response of the detector-preamplifier circuit, and contains no modulation characteristics of the QCL — in short, it should just be the detector responsivity. The value of this responsivity curve at our NICE-OHMS frequency of 387.5 MHz is 15 dB down, corresponding extremely well to the estimates extrapolated from the noise measurements calculated at the beginning of this section. The correspondence of these numbers supports that we have correctly measured the high frequency responsivity function of the detector, assuming the electrical model of the detector is correct.

3.4 Optical Fringing

Another problem that we have observed with the small 100 micron diameter detectors used in the NICE-OHMS experiments is that of optical fringing. Small detectors have to be used because they have low capacitance and hence allow high frequency operation of the detector-preamplifier combination. The problem is that the smaller detector requires significant focusing with a high f-number lens. We have long observed optical fringing in our experiments, but have attributed it to quasi-parallel surfaces elsewhere in the experiment, but we recently discovered that most of the fringing is arising between this cavity transmission detector and its focusing lens. An example of this optical fringing is shown in Figure 3.8, which is reprinted from the FY02 annual report. These curves are results from the direct transmission cavity-enhanced sensor for various operating pressures.

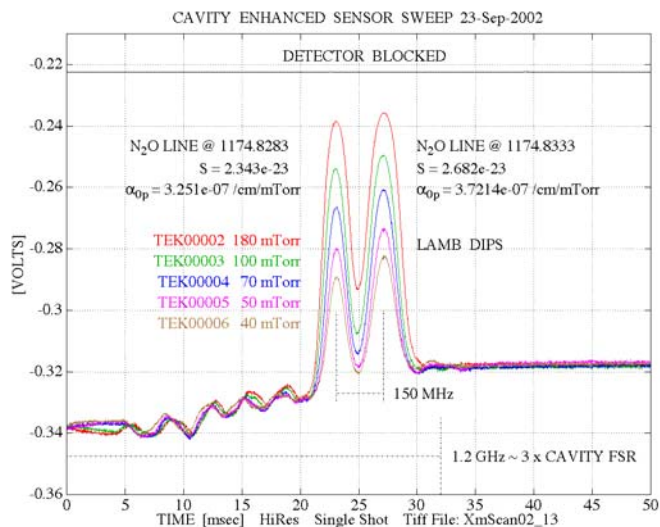


Figure 3.8. Results of Direct Transmission Cavity-Enhanced Sensor. The features at the center of the scans are due to nitrous oxide absorption for various pressures. The smaller features to the left are due to optical fringing — occurring chiefly it was found, between the 100 micron transmission detector and its focusing lens. Reprinted from FY02 report.

The central features are due to nitrous oxide absorption and change with pressure. The features to the left however, do not change with gas pressure and are hence independent of the absorbing medium inside the gas cell: it is due to optical fringing. It is also evident, that the optical fringing features have a similar spectral width as the Doppler-broadened features in the center of the figure as is often the case. Because of this, optical fringing is often the limiting factor in detecting Doppler-limited features with such a sensor. The use of sub-Doppler features such as Lamb dips has the potential to circumvent this problem, but the saturation issue discussed in Section 2, has demonstrated to be severely limiting when using sub-Doppler features. Consequently, it makes sense to consider detecting Doppler-limited spectra as a modus operandi for fieldable cavity-enhanced sensors.

Happily, it has been found that replacing the 100 micron diameter detector with a much larger 1 mm unit greatly reduces this fringing. The 1 mm detector has a fast enough response to do 1-f detection, and so opens the way to make cavity-dithered as well as direct transmission cavity-enhanced sensors.

3.5 Other approaches and Other Detectors

The move to focus on systems other than NICE-OHMS for deployable sensors, involves using larger slower photovoltaic MCT detectors. This does not mean that research into high frequency LWIR detectors will stop. Other approaches to be tried include increasing the bias applied to the detectors. Increasing bias increases the frequency response, but it also increases the noise of the detector. The increased frequency response will result in higher signal levels at high frequency, which will result in increased signal-to-noise provided the noise levels do not rise in a commensurate manner.

Another avenue is that of exploring alternative detectors types. Mercury-cadmium-zinc-telluride (MCZT) detectors are often used as high frequency detectors, and what's more, they operate at room temperature or slightly lower. Various photo-diffusion and photo-electromagnetic MCZT detectors are soon to be tried in our system for evaluation. The predicted problem with these detectors is that while they respond at high frequency, calculations show that it isn't significantly more than that obtained from the current 100 micron MCT detectors, it's just uniform from DC out to high frequency. However, it is a significant advantage that these detectors run room temperature. Since the NICE-OHMS technique yields about the same sensitivity as the 1-f cavity dither technique, this indicates that the reduction in the signal-to-noise due to the lower response of the detector when operating at such high frequency, is compensated for by the corresponding reduction in technical noise. This means that using the NICE-OHMS technique with MCZT may provide a system with approximately equivalent sensitivity to the 1-f cavity dither sensor using the current photovoltaic MCT detectors, but one step closer to room temperature operation.

4.0 QCL Modulation Characteristics

4.1 Modulating QCLs

In general, the amplitude modulation characteristics of QCLs are better than for diode lasers, because QCLs lack the relaxation oscillation that complicates high frequency modulation of diode lasers. This absence of relaxation oscillation was shown by direct modulation of QCLs at frequencies out to beyond 10 GHz with no evidence of relaxation oscillations, which occur in diode laser at about 1-2 GHz. Except at low frequencies where thermal effects dominate, the mechanisms for phase modulation of QCLs by current modulation are not understood. However, we have been able to directly modulate the QCL at 387.5 MHz to produce the phase modulation needed for the NICE-OHMS experiments. QCLs are quite hardy, allowing quite high RF power levels to be applied routinely, for long periods of time with no ill effects. Nevertheless, the modulation properties of QCLs are not perfectly suited to techniques requiring high frequency phase modulation such as NICE-OHMS. Current modulation of a QCL produces both amplitude and phase modulation with a phase shift between them that varies with frequency. This results in residual amplitude modulation producing offsets in some of the signals in the experiment and allowing the coupling of noise into the measurements.

The QCL we have been using for the past two years is one of the early generation lasers (a testament to the reliability of such a device), and perhaps the high frequency modulation characteristics are better in the newer devices. However, we find it difficult to achieve sufficient modulation depth at such high frequencies. Moreover, we are actually running on a resonance in the phase modulation behavior of the device, without which, we would not be able to operate the NICE-OHMS experiment. Figure 4.1 shows the phase modulation spectrum of the device, the resonance at 387 MHz being clearly visible.

We have also observed that such behavior changes laser to laser. In fact, another laser on the same chip as the present one exhibits no resonance at 387 MHz, but a smaller one at 500 MHz. It is unclear what the mechanism is for such a resonance, and its behavior is not well understood at this present time.

The biggest problem the dependence on such a resonance poses to the NICE-OHMS experiment is that the cavity length must be matched to the modulation frequency of the QCL. If the resonance varies from laser to laser to the extent that we have seen, then the cavity length must be quite different for each laser. In addition, such a resonance is quite sharp, so the length matching is critical. We have observed that a difference of half a centimeter has made a difference of a factor of ten or so in signal-to-noise in our experiments.

It is not practical to continue development on a fieldable sensor with these modulation characteristics at this time.

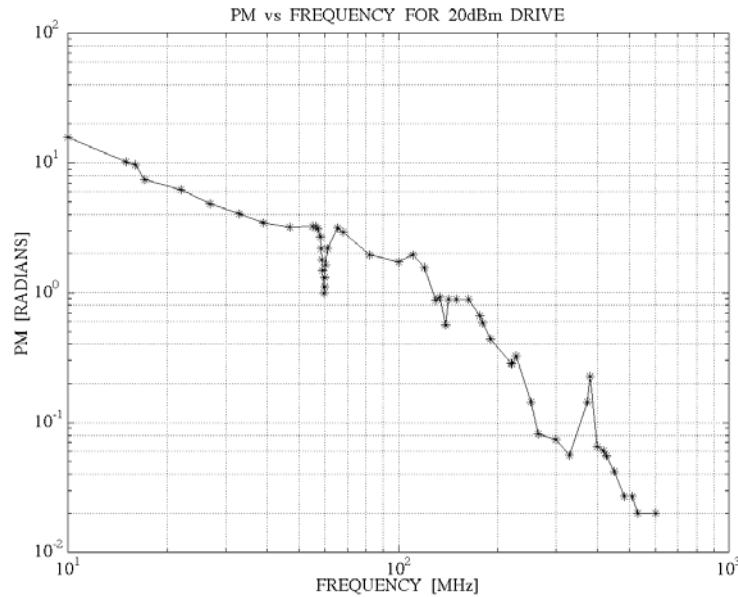


Figure 4.1. Log-Log Plot Showing the Phase Modulation in Radians of the QCL vs. Frequency in MHz for a 20 dBm RF Drive. The resonance at 387 MHz is where we operate the QCL for the NICE-OHMS experiment.

Despite this, we are assured that the modulation performance of QCLs has vastly improved since we obtained our device three to four years ago. The reason why we have not used another device in this particular experiment (apart from resource limitations) is that it overlaps in frequency with another QCL, making it highly useful for some of the laser development work we are doing. For example, the heterodyne measurements of the detectors explained in Section 3.3 could not have been performed without these two overlapping devices.

As we change our focus to the non-NICE-OHMS cavity-enhanced sensors for field deployment, we will continue to use this laser for further testing in this direction. The continued research into the high frequency NICE-OHMS technique and associated detector development will then be able to continue separately and allow us to change out the laser to better explore modulation characteristics of the newer devices.

5.0 FY04 Plans - A Fieldable Sensor

While FY02 was a year of establishing and demonstrating techniques, FY03 was one of identifying limitations and making suitable choices for fieldable sensors. It was found in the attempt to increase the sensitivity of the NICE-OHMS sensor by increasing the cavity finesse, that saturation of the analyte under consideration (nitrous oxide) in the LWIR was a problem when trying to observe sub-Doppler features. It is generally thought that this could be similar if not worse in other analytes. The general conclusions are that while fundamental experiments on the subject will continue, sub-Doppler techniques will not be used as the basis for developing fieldable sensors in the near term. Sensors based on Doppler-limited spectroscopy do not suffer from the same limitation. It was also seen that detector performance in the LWIR needs improving before techniques operating in the hundreds of megahertz can be used without suffering considerable losses. There were some interesting surprises in this work, such as the poorer response of the better frequency-matched detector-preamplifier system. Optical fringing was found to be a problem predominantly when using the smaller area detectors associated with the NICE-OHMS technique, and is not nearly as bad when larger area detectors are used. It was also seen that the modulation characteristics of QCLs are not good and uniform enough at high frequencies to allow the NICE-OHMS technique with modulation frequencies above 100 MHz to become the basis of a reliable fieldable sensor.

In light of the limitations discovered and explored in FY03, a sensible choice for the modus operandi of a fieldable sensor is to use either direct cavity transmission technique (the “Simple Cavity-Enhanced Sensor”), or the cavity-dither FM recovery technique, and target Doppler-limited spectroscopic features rather than sub-Doppler features. In this way, the high frequency modulation and response issues of both the QCLs and the MCT detectors are avoided, and the detector elements can be larger, greatly alleviating the issue of optical fringing. On the other hand, further work will need to be done to correctly estimate the impact of fringing in this case, and most probably to reduce it still further, as it will now be of the same size as the features being targeted. This could possibly involve the implementation of amplitude stabilization as discussed in the introduction, and in the FY02 report. With the use of Doppler-limited features and operation with buffer gas pressures ~ 10 Torr, saturation should not be a problem, and cavity-enhanced sensors of high finesse should be able to operate successfully. However, the impact of saturation in molecules with more than a few heavy atoms (not hydrogen) needs to be examined.

It is also imperative that research into the NICE-OHMS technique be continued. A lot of the limitations discussed in this report can be overcome as technology advances, a better understanding is gained of the behavior of available detectors, and perhaps with use of folded optical cavities. In particular, it is proposed that PNNL work closely with companies like Fermionics on these issues. With the resources PNNL now has available, we could help such companies characterize the performance of their detectors in ways that they haven't yet been able to, such as the high frequency heterodyne technique discussed in Section 3.3.

6.0 References

Demtröder W. 1996. *Laser Spectroscopy, Basic Concepts and Instrumentation*, 2nd Ed., ISBN 3-540-57171-X, Springer-Verlag, Berlin, Heidelberg, New York.

Gianfrani L, RW Fox and L Hollberg. 1999. *J. Opt. Soc. Am. B*, **16**(12):2247.

Ishibashi C and Hiroyuki Sasada. 1999. *Jpn. J. Appl. Phys.* **38**:920.

Taubman MS, TL Myers, BD Cannon, RM Williams and JF Schultz. 2003. *Ultra-Trace Chemical Sensing with Long-Wave Infrared Cavity-Enhanced Spectroscopic Sensors*. PNNL-14201, Pacific Northwest National Laboratory, Richland, WA.

Ye J, L-S Ma and JL Hall. 1998. *J. Opt. Soc. Am. B*, **15**(1):6.

Appendix A

Further Work for FY03 - Taken From the FY02 Report

Appendix A

Further Work for FY03 - Taken From the FY02 Report

Several improvements to the cavity-enhanced sensors are already underway. FY03 will see the construction of better optical cavities and gas handling systems for use in our chemical sensor experiments. This will involve better mirrors, better acoustic damping, better vacuum pumps, better pressure measurements, and lower contamination from out gassing and leaks for a more complete exploration of the performance of the NICE-OHMS sensor. This is important, because the most convincing demonstration of the sensitivity of a sensor is with absorptions near the noise limit and not by extrapolating by two orders of magnitude based on signal-to-noise ratio. Mirrors of higher reflectivity and very low loss are now becoming more available in the LWIR due in part to PNNL's interaction with certain coating houses. The resulting increase in cavity finesse will increase our access to weak absorption lines and enable us to detect lower concentrations of analytes in test samples. New mounting arrangements using better piezoelectric electric actuators will hopefully allow longer scan ranges and increase the utility of the instrument.

Certain fundamental changes in design will also be tested including the implementation of amplitude stabilization as discussed in 3.2 (of Taubman et al. 2003) to aid in the reduction of fringing. To completely eliminate the effects of optical fringing, redesign of the optics in the path ways between the cavity and both the reflection and transmission detectors will be necessary in addition to amplitude stabilization. It is unlikely a complete redesign of the optics will be completed in FY03, but at least work with a ring cavity will be started. A change to higher reflectivity cavity mirrors will likely require addition of an additional servo control loop to maintain the correct NICE-OHMS RF modulation frequency. This has not yet been necessary because the cavity bandwidth has been large enough to allow adjustment of this modulation frequency, but manual adjustment may no longer be adequate with higher finesse values. For example, tuning the cavity over 1.2 GHz or three times the FSR changes the cavity length by 1 part in 30,000. This is small relative to the 1 part in 2415 that the cavity bandwidth is as a fraction of the FSR. However, with increased finesse and/or increased scan lengths, the change in the FSR with scanning will become comparable or larger than the cavity bandwidth.

There are disadvantages to continuously increasing the cavity finesse, and in FY03 we may be at the point where we can investigate these limits. The extra servo loop mentioned above will operate at a low frequency, probably in the 100s of Hz. This will decrease the required measurement bandwidth, or conversely, increase the necessary averaging time to remove the ripple resulting from this extra modulation. The resulting longer measurement times may actually prove disadvantageous. In addition to this, the frequency of the cavity-dither modulation may have to be reduced because of the increased cavity finesse and interference with the cavity mode via the Doppler effect of the moving mirror as discussed in Section 2.4.1 (of Taubman et al. 2003), forcing the frequency of the extra modulation described above to be reduced even further. It will be of prime importance to see what sensitivity the

instrument has, and what concentrations of which species are available at this sensitivity when this limit is reached. The experimental investigation of the performance of the sensor with higher finesse mirrors will be accompanied by an attempt to gain a better understanding of the theory of the disruption of the cavity mode due to mirror motion, although it is unclear whether a full theory will be developed by the end of FY03.

Appendix B

Frequency Control Loop in NICE-OHMS Experiments

Appendix B

Frequency Control Loop in NICE-OHMS Experiments

In the ultimate form of any NICE-OHMS system, there is a separate servo loop used specifically to lock the modulation frequency to the FSR of the optical cavity. This is because as the cavity is scanned, the FSR changes slightly, necessitating a slight adjustment in the NICE-OHMS frequency.

This loop would operate in the same manner as all control loops, requiring a dither modulation of the actual NICE-OHMS modulation frequency, and the generation of an error signal proportion to the frequency difference between the NICE-OHMS modulation frequency and the cavity FSR. This error signal in turn would drive a servo unit to change the frequency of the oscillator providing the NICE-OHMS modulation signal.

Apart from the extra complexity added to a system already containing three separate modulation systems and one precision locking loop, there are two significant side effects of adding such a loop, compared to a system that can run with it, as our system does currently. The most important of these is that measurement times would increase significantly. This is due to the extra averaging time necessary to filter out the fluctuations arising from the modulation of the NICE-OHMS frequency, necessary for the operation of this servo loop.

This secondary modulation frequency could not be higher than a kilohertz or so, and would most probably be in the hundreds of Hertz. To obtain smooth profiles of the molecular lines observed by the NICE-OHMS detector, this would require considerably more averaging and/or low pass filtering. In turn, this reduced bandwidth would result in considerably slower sweep rates to avoid signal loss and distortion. With the cavity finesse values used at PNNL in FY02 (2415), there is no need for an automated system to maintain the NICE-OHMS frequency with that of the cavity FSR. Specifically, the linewidth was 160 kHz. The linear change in FSR over the current tuning range of 1.5 GHz is 16.5 kHz, being roughly a tenth of the cavity linewidth. A sensor could operate under these conditions without full active tuning, or even relying on manual calibration. Simple computer-based tuning during a calibration stage would be all that was necessary.

The beauty of not including this active tuning loop, is that the sensor can scan at hundreds of Hertz, the lowest frequency fluctuations requiring filtering being the cavity dither at around 60 kHz, making it possible that the sensor could gain meaningful high signal-to-noise data in a fraction of a second. Including such a loop may increase the measurement times to many seconds or even minutes.

Distribution

**No. of
Copies**

**No. of
Copies**

OFFSITE

Mr. W. Randy Bell
 United States DOE
 NNSA/NA-22
 1000 Independence Ave. SW
 Washington, DC 20585

Dr. David Berry
 United States DOE
 NNSA/NA-22
 1000 Independence Ave. SW
 Washington, DC 20585

LTC John C. Carrano, PhD
 Program Manager
 DARPA, MTO
 3701 N. Fairfax Dr.
 Arlington, VA 22203-1714

Mr. Ralph Hastings
 United States DOE
 NNSA/NA-22
 1000 Independence Ave. SW
 Washington, DC 20585

Mr. Eric Sanders
 United States DOE
 NNSA/NA-22
 1000 Independence Ave. SW
 Washington, DC 20585

Dr. Vaughn Standley
 United States DOE
 NNSA/NA-22
 1000 Independence Ave. SW
 Washington, DC 20585

ONSITE

44 Pacific Northwest National Laboratory

Aker, PM	K5-25
Bonebrake, CA	K5-25
Cannon, BD	K5-25
Doherty, TJ	K8-09
Harper, WW	K5-25
Johnson, BR	K6-24
Myers, TL	K5-25
Schultz, JF (26)	K5-25
Sheen, DM	K5-25
Stewart, TL	K5-25
Taubman, MS	K5-25
Wojcik, MD	K5-25
Information Release Office (7)	K1-06